Journal of Thermal Analysis and Calorimetry, Vol. 96 (2009) 2, 353–361

IRON ORE SINTERING
Characterization by calorimetry and thermal analysis

*Riham Michelle Morcos and Alexandra Navrotsky**

Peter A. Rock Thermochemistry Laboratory and NEAT ORU, University of California at Davis, Davis, CA 95616, USA

Differential scanning and high temperature reaction calorimetry have been used to characterize a series of natural iron ore and flux samples commonly used during iron ore sintering. Most iron ore samples were shown to contain measurable quantities of goethite, with a characteristic dehydration peak in DSC and TG between 200 and 400°C. At higher temperatures, all samples decomposed to produce magnetite with an accompanying mass loss in the TG profile due to the evolution of oxygen.

High temperature reaction calorimetry has been used to measure the heat of solution of the ore in the melt formed during iron ore sintering. The dehydration and calcination of iron ore and flux samples was also examined using high-temperature reaction calorimetry. The results support the DSC/TG findings.

Keywords: *DSC, hematite, iron oxide melts, thermal analysis*

Introduction

Within an integrated steelworks, the role of the sinter plant is to supply the blast furnace with sinter of consistent chemical and physical properties. Parameters such as quality – a general term that is used to describe the performance of the sinter in the blast furnace – and yield are largely determined by the structure of the sinter, and the phases that precipitate on cooling [1–3]. Properties of the melt, such as viscosity, density and surface tension, which all influence the level of assimilation and pore/bubble coalescence during sintering, are not only dependent on chemical composition, but also and the degree of superheat. For this reason, the thermal properties of the raw materials used during sintering, namely iron ore and fluxes, are of particular interest [4–6]. To this end, simultaneous differential scanning calorimetry (DSC) and thermogravimetric analysis (TG) together with high-temperature reaction calorimetry have been used to characterize a series of naturally occurring iron ores and fluxes commonly used in ironmaking.

High temperature reaction calorimetry has been very useful for studying melt thermodynamics. In particular, transposed temperature drop calorimetry, which involves dropping a sample at room temperature into an empty hot calorimeter, and drop solution calorimetry, which involves dropping a sample at room temperature into a molten solvent inside a hot calorimeter, have been used to directly measure heats of fusion and of solution up to 1500°C [7–10]. The high temperature capabilities of these techniques and the obvious analogies of drop solution calorimetry to the process of nuclear assimilation during sintering make these methods ideal for quantifying the thermodynamics of the fundamental processes occurring during iron ore sintering. This study examines the thermodynamic properties of a series of naturally occurring iron ores and fluxes commonly used during iron ore sintering. To simulate the process of particle assimilation during sintering, the dissolution of the ores into an iron-rich melt was examined using high-temperature reaction calorimetry.

Experimental

Sample preparation

The calorimetric solvent (Solvent 1) was prepared by mixing stoichiometric quantities of high purity (>99%) analytical grade reagents in a mortar and pestle to a composition 73.89 mass% Fe_2O_3, 18.79 mass% $CaCO_3$, 4.55 mass% SiO_2, 1.9 mass% Al_2O_3 and 0.88 mass% MgO. This sample represents the initial composition of the –0.5 mm size fraction of a typical JKT (Japan–Korea–Taiwan) sintering blend.

A selection of eight iron ore fines (–8 mm) from Australia, Brazil, India and South Africa was examined. The ores were dried in an oven overnight before being crushed to approximately 2 mm in a roll crusher and milled to below 100 micron using a ring mill. For DSC, the full size distribution (–8.0 mm) was crushed and milled, while for high temperature reaction calorimetry (TTD and DS) only the +0.5 mm size fraction was crushed and used. This was done to examine the assimilation of particles into the melt.

* Author for correspondence: anavrotsky@ucdavis.edu

1388–6150/$20.00

Akadémiai Kiadó, Budapest, Hungary
Springer, Dordrecht, The Netherlands

The chemical compositions of the ores are given in Table 1. Sample S1 is a Brockman hematite ore from Australia. It is predominately hematite with only small amounts of goethite. It contains approximately 2.2% alumina in the form of kaolinite. Sample S2 is a Marra Mamba ore from Australia. It is higher in goethite than sample S1 with a hematite to goethite ratio of 2:3. Samples S3 and S4 are pisolite ores from Australia. They have high levels of goethite and low alumina. Samples S5 and S6 are dense hematite ores from Brazil. They are higher in iron and lower in gangue minerals compared to the ores from Australia. Sample S7 is a hematite-goethite ore from the Chowgule region in India. It is high in both silica and alumina compared to ores from Australia and Brazil. Sample S8 is a dense hematite ore from South Africa. It is high in iron and has a low loss on ignition (LOI). Similar to the iron ores, the fluxes were dried in an oven at 1000°C overnight before being crushed and milled to a size below 100 microns.

Methods

Differential scanning calorimetry

To measure the volatile content of the iron ore and flux samples, thermogravimetry (TG) and differential scanning calorimetry (DSC) were conducted using a Netzsch simultaneous thermal analyzer, (STA 449). A 30 mg pellet of powder was packed in a standard alumina crucible with a lid inside. The loaded crucible was placed in the DSC and heated from room temperature to 100°C and held for 1 h before heating to 1400°C at 20°C min^{-1} in an argon atmosphere. Subsequently, the sample was cooled from 1400°C to room temperature at 20°C min^{-1}. The DSC scan was repeated (with a fresh charge) for each sample to check for reproducibility. Baseline correction was completed using an earlier scan of the empty alumina crucible under the same conditions. The temperature was calibrated against the melting point of several metal standards (In, Bi, Zn, Al and Au), and sensitivity calibrations were preformed using the heat capacity of sapphire.

Powder XRD

The XRD measurements were performed using an Inel diffractometer operated at 30 A and 30 keV with CoK_α radiation and calibrated using quartz as a standard. Data were collected in the 2θ range from 10 to 90°. Cell parameters and mass ratios of the crystalline phases (for recovered S5a after TTD) were refined from XRD patterns using a whole profile (Rietveld)

Table 1a Initial composition of iron oxide samples and melts used in calorimetry (mass%)

Sample	Fe	CaO	SiO_2	Al_2O_3	MgO	P	Mn	LOI	Total
S1	63.30	0.06	4.07	2.18	0.11	0.03	0.09	2.70	72.54
S2	62.13	0.01	2.99	1.88	0.06	0.06	0.17	5.58	72.88
S3	58.22	0.04	5.18	1.40	0.06	0.04	0.02	9.77	74.73
S4	56.78	0.19	4.77	1.72	0.05	0.05	0.03	11.61	75.20
S5	66.39	0.03	1.24	1.09	0.03	0.02	0.36	2.07	71.23
S6	65.39	0.04	3.65	0.91	0.03	–	–	0.96	70.98
S7	61.71	0.02	4.21	2.10	0.60	–	–	4.12	72.76
S8	65.37	0.09	3.73	1.50	0.04	–	–	0.54	71.27
S9	0.59	54.10	0.90	0.32	0.55	–	–	43.12	99.58
S10	0.54	30.31	1.04	0.34	20.60	–	–	46.62	99.45
S11	5.57	2.05	41.30	1.82	36.15	–	–	9.96	96.85
S1a	63.30	0.06	4.07	2.18	0.11	0.07	0.09	2.70	72.58
S2a	62.13	0.01	2.99	1.88	0.06	0.06	0.17	5.58	72.88
S3a	58.22	0.04	5.18	1.40	0.06	0.04	0.02	9.77	74.73
S4a	56.78	0.19	4.77	1.72	0.05	0.05	0.03	11.61	75.20
S5a	66.39	0.03	1.24	1.09	0.03	0.02	0.36	2.07	71.23
S10a	0.54	30.31	1.04	0.34	20.60	–	–	46.62	99.45
S11a	5.57	2.05	41.30	1.82	36.15	–	–	9.96	96.85

Table 1b Initial composition of iron oxide solvent used in calorimetry (mass%)

Solvent	Fe_2O_3	$CaCO_3$	SiO_2	Al_2O_3	MgO	Total
Solvent 1	73.89	18.79	4.55	1.9	0.88	100.0

fitting routine found in Jade analysis software. Powder simulation patterns form the ICSD database [11] were used as references for phase identification.

High temperature calorimetry at 1353°C

High temperature calorimetry at 1353°C was used to measure the heat of transposed temperature drop and drop solution in air. The calorimeter used (Model HT-1500, Setaram, Caluire, France) was the same as that in previous studies [8–10, 12–15]. In the transposed temperature drop calorimetry (TTD) experiment, a loosely pressed pellet of powdered sample was dropped into a hot calorimeter in the absence of solvent. The heat effect is equal to the heat content of the sample, $\int_{298}^{T} C_p \mathrm{d}T$, if no phase transformation or decomposition occurs. The TTD experiment yields heat content plus the enthalpy of decomposition and/or fusion (when these occur). The drop solution experiment involves dropping a sample pellet from room temperature into a solvent held at calorimeter temperature. The heat effect is equal to the heat content plus the enthalpy of solution at calorimeter temperature, plus the enthalpy of any gas evolution or oxidation–reduction reactions, if present.

$$\Delta H_{ds} = \Delta H_{so\,ln} + \int_{298}^{T} C_p \mathrm{d}T \qquad (1)$$

About 0.70 g of the solvent (starting with a powder mixture) was placed in a platinum sample crucible, loaded into the calorimeter, and heated to operating temperature. The solvent was molten and had relatively low viscosity at the calorimeter temperature. The operating furnace temperature was 1385°C and the corresponding calorimeter temperature was 1353°C.

For instrument qualification, the heat content of α-Al_2O_3 and α-Fe_2O_3 were measured to verify the calibrations. TTD calorimetry was performed by dropping 5 or 15 mg pellets of samples into an empty Pt crucible using the same calorimeter and operating conditions. The calibration factors for the calorimeter (J mV^{-1}) were obtained by dropping platinum pieces. Platinum calibration pieces were dropped alternately with the alumina for the initial tests. This overall methodology is now standard and has been reported previously [10, 16]. The calibration factors showed no systematic variation with subsequent pellet drops. The errors in enthalpy of drop solution at 1353°C were ±5%, considering both the scatter of the data and the standard deviation of the platinum calibration. A series of samples were dropped in the standard solvent described above (Solvent 1). Several pellets of the same composition were dropped into a batch of solvent Fresh solvent was used for each new sample. The total mass of sample pellets dropped was approximately half the mass of the solvent (1:2 sample/solvent ratio). The solubility and rate of dissolution of samples were checked in 0.70 g batches of a series of iron rich melts in a platinum crucible at 1353°C in a furnace. In all cases except the two samples S1a and S5a, the pellets dissolved completely within 10 min.

High temperature calorimetry at 702°C

To further examine the dehydration of goethite and other reactions, high-temperature drop solution and transposed temperature drop calorimetry was performed in a custom built Tian–Calvet microcalorimeter. The calorimeter measures heat flow through a sensitive thermopile, which surrounds the sample chamber and separates it from a large alloy block maintained at a constant temperature of 702°C. The calorimeter and standard procedures have been described previously [7, 17]. A 15 mg pellet was dropped from room temperature into molten lead borate ($2PbO–B_2O_3$) solvent at 702°C. Oxygen gas was simultaneously flushed over the solvent at 100 mL min^{-1} to maintain an oxidizing atmosphere in the calorimeter. The calorimetric signal was recorded as a voltage change in the thermopile *vs.* time. The area under the curve was proportional to the heat effect. The integrated voltage *vs.* time curve was converted to enthalpy by application of a calibration factor based on the heat content of α-Al_2O_3 pellets of similar mass as the glass samples. All the calorimetric runs of iron ore samples returned to baseline in approximately 50 min. This time is characteristic of the calorimeter's time constant and the shapes of the curves suggest complete dissolution in less than 10 min.

Results and discussion

Characterization

DSC analysis

Upon heating, the DSC/TG profiles of iron ore samples S1–S5 and sample S7 show an endothermic peak in the range 200–350°C (Fig. 1). Note that Fig. 1 shows samples S1–S5 and the remaining DSC/TG profiles are found elsewhere [18]. This peak is due to the dehydration of goethite, with an associated mass loss in the TG scan. In samples S5 and S7 this peak appears as an endothermic double peak. Similar endothermic double peaks have previously been reported for Brazil and India iron ores [19], and recent work has suggested this may be related to the size distribution of the goethite crystals [20]. For iron ore samples S6 and S8, while it was not possible to identify a dehydration peak within the DSC scan, there was some mass loss at 200–400°C that may be due to the dehydration of small quantities of goethite. These results is consistent with the data in Ta-

ble 1, which show samples S6 and S8 have the lowest LOI of all the iron ores examined (LOI<1.0%). In all iron ore samples, the dehydration of gangue minerals such as gibbsite or kaolinite could not be identified from the DSC or TG scans.

At higher temperatures, a sharp endothermic peak was visible for all iron ore samples. This peak is attributed to thermal reduction of hematite to magnetite, which becomes spontaneous at temperatures above 1000°C.

The DSC/TG profiles of samples S9 (limestone), S10 (dolomite) and S11 (serpentine) show a 43.2, 46.4 and 9.9% mass loss, respectively (published elsewhere) [18]. A summary of the DSC/TG profiles (enthalpy of transition ΔH_{trns} for peaks 1 and 2 and the total mass loss) for iron ore and flux samples is presented in Table 2. Using the calculated molecular mass for sample S3 (159.7 g mol^{-1}), the enthalpy of dehydration was estimated from the DSC scan to be 47.3 kJ mol^{-1}. This value is reasonably close to the value (39.4±1.1 kJ mol^{-1}) measured using drop solution calorimetry at 702°C (see below) and the work of previous authors [20].

XRD analysis

XRD analysis was performed on selected samples to examine the transformations that took place inside the calorimeter. The XRD patterns of sample S5a both before and after heating during the TTD experiment

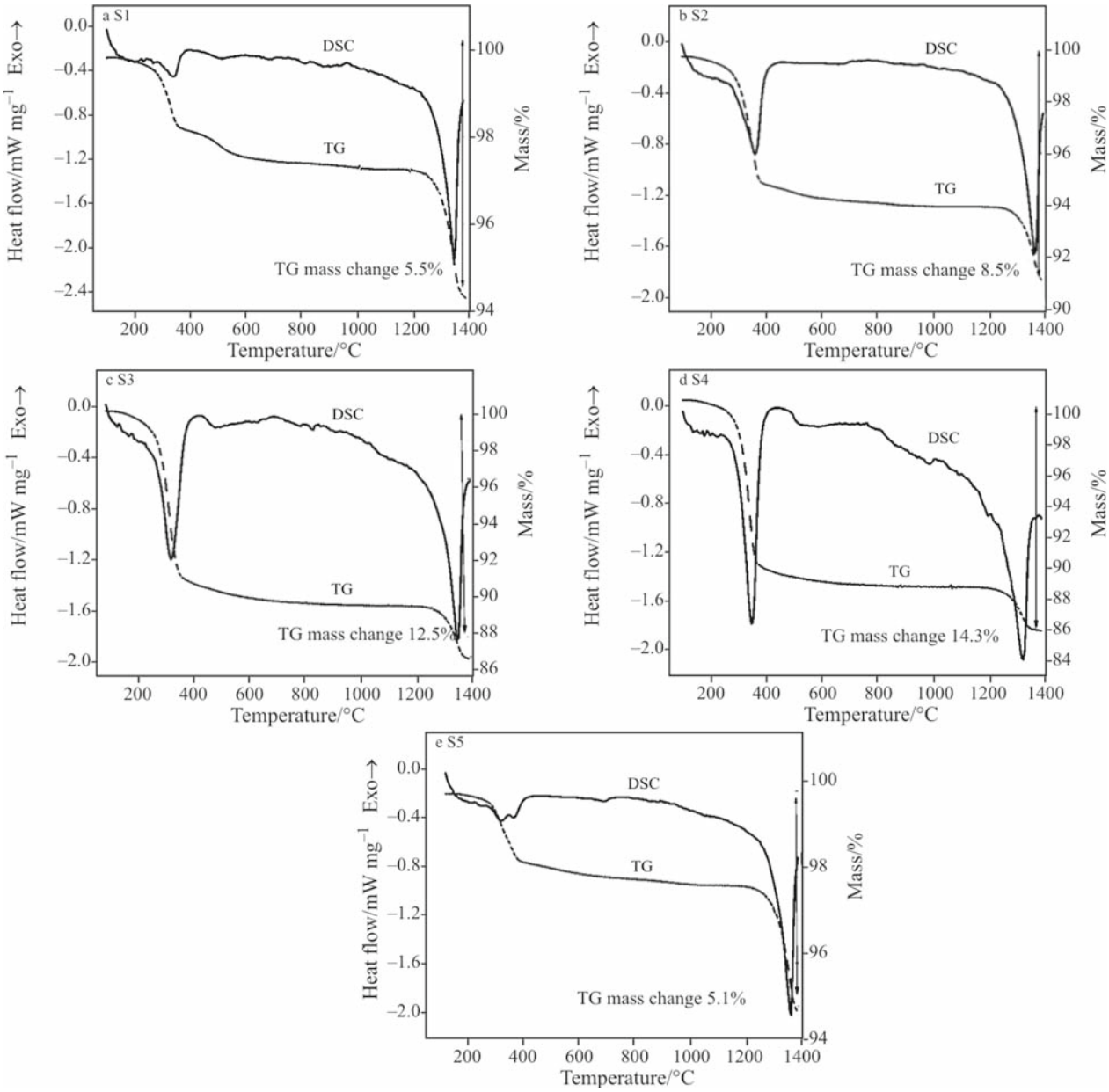

Fig. 1 DSC/TG profiles of sample a – S1, b – S2, c – S3, d – S4, e – S5.

are displayed elsewhere [18]. For the initial material, the XRD pattern agrees well with that of hematite, Fe_2O_3 (literature (ID-64-5075) [21]. The Fe_2O_3 has the following lattice parameters, a=b=5.0380 and c=13.7720 Å and approximate particle size of 300 nm. The heat-treated sample of S5a (S5aS) recovered from the Pt crucible after heating to 1353°C) has strong Fe_2O_3 and Fe_3O_4 (hematite and magnetite) peaks. Rietveld refinement [22] yields 84 mass% (73 mol%) magnetite and 16 mass% (27 mol%) hematite. Therefore, after heat treatment the iron ores are at least partially reduced from hematite to magnetite, as has been reported in other iron oxide systems [23–25]. It is possible that a greater extent of reduction occurred at high temperature, with some re-oxidation during cooling in the calorimeter. XRD measurements on samples S5a and S4a, identified only hematite, magnetite, and goethite. The other components in the sample (SiO_2, Al_2O_3, MgO, CaO, P_2O_5 and MnO_2) represent less than 5 mass% of the mixture and therefore those phases (if present) could not be identified in XRD measurements. In addition, XRD is insensitive to moderate amounts of glassy or amorphous phases.

High temperature calorimetry at 1353°C

Drop solution experiments

The heat of drop solution was measured for iron ore (S1a–S5a) and flux (S10a and S11a) samples in Solvent 1 (Tables 3a kJ mol^{-1}; 3b kJ g^{-1}). The solvent represents the chemical composition of a typical primary melt formed during the initial stages of sintering. The heats of drop solution for the iron ore samples are almost constant (within error), in the range 1390 to 1593 J g^{-1}. As expected, the ores with higher LOI show slightly higher heats of drop solution, as this figure includes not only the energy to assimilate the particle into the melt, but also the energy to dehydrate any goethite present in the sample. After completion of the drop solution experiments, the measured mass loss for samples S1a and S5a was ~2 mass%, while samples S2a, S3a and S4a showed an ~8 mass% loss. The mass loss observed in the latter samples is larger since these samples contain more chemically bound water (in FeOOH) and is in agreement with the DSC/TG profiles in Fig. 1. Incomplete dissolution was observed for samples S1a and S5a.

TTD experiments

In TTD experiment, a pelletized powdered sample was dropped into a hot calorimeter in the absence of solvent. The heat effect is equal to the heat content of the sample, if no phase transformation or decomposition occurs. The TTD experiment yields heat content plus the enthalpy of oxidation, reduction, decomposition and/or fusion (when these occur). The H_{TTD} values of samples S1a–S5a, and Solvent 1 determined by dropping 15 mg pellets into an empty crucible at 1353°C are shown in Table 3. The H_{TTD} of Solvent 1, 231.8±6.8 kJ mol^{-1}, is in good agreement with earlier studies [14, 15].

For the iron ores, samples S1a and S5a show significantly larger H_{TTD}, 374 and 392 J mol^{-1}, respectively, compared to ores S2a–S4a (265–286 J mol^{-1}). After the TTD experiments, it was found that samples S1a and S5a did not form a melt in the calorimeter, whereas samples S2a–S4a had melted completely; the former showed evidence of pellets, the latter a layer of material with a smooth surface. These observations help

Table 2 Summary of DSC/TG profiles for iron ore samples. The enthalpy of transition ΔH_{tr} for (peaks 1, 2, respectively) and the total mass loss of the sample

Sample	Temp./°C peak 1*	Temp./°C peak 2*	ΔH_{tr}/J g^{-1} for peak 1*	ΔH_{tr}/J g^{-1} for peak 2*	Peak 1 dehydration TG/%	Total TG %
S1	334.0	1343.1	32.41	169.48	1.50	5.47
S2	360.1	1359.7	122.54	137.61	4.92	8.48
S3	329.4	1345.1	296.46	263.26	8.69	12.53
S4	345.3	1317.5	245.27	230.27	10.53	14.32
S5	300.5	1362.1	28.06	145.97	1.53	5.06
S6	325.3	1339.3	–	584.60	0.68	3.93
S7	340.0	1322.8	196.02	598.07	3.44	8.68
S8	222.6	1348.2	–	223.98		3.65
S9		894.3		1673.3		43.16
S10	797.3	888.1	1512.52[a]			46.41
S11	744.3	830.6	348.83[a]			9.89

*Peak 1 and peak 2 refer to the low temperature and high-temperature peaks respectively, as shown in Fig. 1 (a–L). [a]Combined enthalpy of transition for both peaks 1 and 2

Table 3a Summary of transposed temperature drop experiments ΔH_{ttd} and heat of drop solution ΔH_{ds}, and heat of solution ΔH_{soln} (kJ mol^{-1})

Sample	ΔH_{TTD}/kJ mol^{-1}	$\Delta H_{TTD\ (corrected)}$/kJ mol^{-1}	ΔH_{ds}/kJ mol^{-1}	ΔH_{soln}/kJ mol^{-1}
Solvent 1	231.8±6.8 (7)	–	–	–
S1a	373.6±10.2 (7)	280.5±10.2	198.0±2.3 (6)	–
S2a	285.8±4.6 (5)	–	223.3±5.0 (6)	–62.5±6.8
S3a	265.2±3.7 (7)	–	219.3±4.51 (7)	–46.0±5.8
S4a	279.9±15.8 (7)	–	221.7±7.9 (8)	–58.3±17.7
S5a	392.3±9.3 (7)	285.4±9.3	203.7±7.0 (10)	–
S10a	107.5±0.4 (7)	–	–	–
S11a	96.6±4.3 (8)	–	106.0±1.0 (8)	9.4±4.4

*Uncertainty is two standard deviations of the mean. The number in parentheses is the number of experiments

Table 3b Summary of transposed temperature drop experiments ΔH_{ttd} and heat of drop solution ΔH_{ds}, and heat of solution ΔH_{soln} (J g^{-1})

Sample	ΔH_{TTD}/J g^{-1}	ΔH_{ds}/J g^{-1}	ΔH_{soln}/J g^{-1}
Solvent 1	1776.9±52.4 (7)	–	–
S1a	2622.0±60.7 (7)	1389.5±16.0 (6)	–
S2a	1955.2±26.4 (5)	1527.6±34.4 (6)	–427.6±43.4
S3a	1893.7±24.1 (7)	1577.4±32.4 (7)	–316.3±40.4
S4a	2044.0±103.3 (7)	1593.2±56.9 (8)	–450.8±117.9
S5a	2506.4±56.0 (7)	1429.6±42.7 (10)	–
S10a	2206.0±29.3 (7)	–	–
S11a	1861.0±77.0 (8)	2042.1±16.5 (8)	78.7±43.4

*Uncertainty is two standard deviations of the mean. The number in parentheses is the number of experiments

explain the observed pattern of enthalpies. These and previous experiments suggest that samples which melt completely retain most of their iron as Fe^{3+}, while samples retaining solid phases have substantial reduction of hematite to magnetite. The H_{TTD} values of samples S2a, S3a and S4a are essentially the same since their compositions are very similar. The final state of samples S2a, S3a and S4a in the calorimeter remains oxidized since the samples melted and the melt remains oxidized. Both samples S1a and S5a did not melt completely and have a significantly larger H_{TTD}/values due to the endothermic reduction of hematite to magnetite. However, when magnetite dissolves in the ore melt, it then oxidizes (with an exothermic heat effect) back to mainly ferric iron. Our data (calorimetry, mass loss and X-ray diffraction) suggest that the hematite in samples S1a and S5a in the calorimeter was largely reduced to magnetite (these samples remained as solid pellets).

The significantly higher values of H_{TTD} recorded for samples S1a and S5a, is due to the reduction of hematite to magnetite inside the calorimeter. In order to compare TTD data for these samples, it is necessary to correct for the reduction from hematite to magnetite. Two methods are described below:

Method 1: TTD Correction by using TG (mass loss) data

After TTD measurements, 15 mass% loss was measured for sample S5a. Both samples S5 and S5a have approximately the same composition. The DSC/TG scan for sample S5 shows two mass loss regions, 1 mass% at 350°C for loss of surface water and/or combined water and 3.5 mass% at 1360°C for reduction of hematite to magnetite (total of 5 mass%). If we use the mass loss measured by DSC/TG, the following corrections can be made. The weighted average molecular mass for sample S5a is 153.4 g mol^{-1}. Assuming the 3.5 mass% loss at 1360°C accounts for the reduction of Fe^{3+}; then 153.4 g·0.035=5.369 g (equivalent to 5.369 g/32 g mol^{-1} O_2=0.168 mol O_2) of oxygen is evolved. The enthalpy of reaction (reduction) can be expressed as the following:

$$3Fe_2O_3 \rightarrow 2Fe_3O_4 + 0.5O_2 \quad (2)$$

$$\Delta H_{rxn} = 2\Delta H_f^0\ (Fe_3O_4) + 0.5\Delta H_f^0\ (O_2) - 3\Delta H_f^0\ (Fe_2O_3) \quad (3)$$

The literature values for ΔH_f^0 of hematite, magnetite and calculated ΔH_{rxn} (reduction of Fe_2O_3 to Fe_3O_4)

are found in Table 4. The ΔH_{rxn} are 247.2±2.5 kJ mol^{-1} at 25°C and 249.8±2.5 kJ mol^{-1} at 1353°C, respectively.

One mole O_2 corresponds to 6 moles of Fe_2O_3. Consequently, the total moles of Fe_2O_3 is equal to 6·0.168 mol=1.00 mol Fe_2O_3. Therefore, it is safe to assume that at high temperature (1353°C) essentially all Fe_2O_3 is reduced to Fe_3O_4. Using this calculation method for sample S5a, the $\Delta H_{TTD\ (corrected)}$ = H_{TTD}–mol% Fe_2O_3·(ΔH_{rxn}/3 mol Fe_2O_3)=392 kJ mol^{-1} –1.00 mol Fe_2O_3 (249.8 kJ mol^{-1}/3)=308.18± 15.4 kJ mol^{-1}. This $\Delta H_{TTD\ (corrected)}$ of 308 kJ mol^{-1} is roughly the same (within error) as the H_{TTD} values reported for samples S2a, S3a and S5a.

Method 2: TTD correction by using XRD measurements

Sample S5a contained 93 mol% hematite, of which 73 mol% hematite was reduced to magnetite during the TTD experiment. The corrected $\Delta H_{TTD\ (corrected)}$ can be expressed as:

$$\Delta H_{TTD\ (corrected)} = \Delta H_{TTD} - \text{mol } (Fe_2O_3 \text{ to } Fe_3O_4)\% \text{ reduced} \cdot \Delta H_{rxn} \quad (4)$$

The larger measured endothermic ΔH_{TTD} value is reasonable considering the reduction of Fe_2O_3 to Fe_3O_4 is strongly endothermic. Using the above expression, $\Delta H_{TTD\ (corrected)}$ values for S1a and S5a are 280.5 and 285.4 kJ mol^{-1}, respectively. The corrected $\Delta H_{TTD\ (corrected)}$ value for samples S1a and S5a are in good agreement with those for the other samples S2a, S3a and S4a).

Heat of solution

The heat of solution H_{soln} is determined by

$$\Delta H_{soln,1353°C} = \Delta H_{ds,1353°C} - (H_{1353°C} - H_{25°C}) \quad (5)$$

The heat of solution of samples S2a, S3a and S4a, (obtained by subtracting the heat content of the sample) is shown in Table 3. Fe_2O_3 saturation was not achieved for these experiments. Saturation would be suspected when (1) heat of drop solution would approach the heat content values or (2) reaction time would increase, indicating slower dissolution. Neither was observed. All H_{soln} values for samples S2a, S3a and S4a are strongly exothermic and the same (within experimental error). After the heat of drop solution experiment was measured for samples S1a and S5a, partially dissolved pellets were found in the Pt crucible (it is noted that both samples S1a and S5a do not melt under experimental conditions). Therefore, the H_{soln} of samples S1a and S5a have not been calculated since partial dissolution occurred.

In previous calorimetric studies, the H_{soln} (54 kJ mol^{-1}) was strongly endothermic for hematite dissolution in iron rich melts [14]. However, in this study, we measured H_{soln} (–55 kJ mol^{-1}) that was strongly exothermic. Indeed, this measured exothermic H_{soln} agrees with our earlier hypothesis of oxidation-reduction reactions for two reasons. First, H_{TTD} of samples S2a, S3a and S4a are very endothermic, predominately due to hematite reduction to magnetite. Second, in the drop solution experiments, the sample remained mainly oxidized when dissolved in the solvent and reduction of hematite is thus not an issue. Therefore, in the drop solution experiments, the samples are much less reduced than in transposed temperature drop experiments. If the heat effect due to hematite reduction to magnetite (107 kJ mol^{-1}) is added to the H_{soln} (–55 kJ mol^{-1}) value, our corrected H_{soln} (52 kJ mol^{-1}) becomes endothermic and in agreement with previous results of hematite dissolution in typical iron rich melts.

High temperature calorimetry at 702°C

Heat of solution and heat of dehydration

We used the custom built Tian–Calvet calorimeter operating at 702°C for these experiments since this temperature, at which our calorimeter routinely operates, is one after goethite dehydration occurs and before the reduction of hematite to magnetite.

The enthalpy of dehydration of iron ore sample S3 can be calculated through the thermochemical cycle in Table 5. A summary of the calorimetric results; enthalpies of transposed temperature drop (ΔH_{TTD}) and enthalpies of drop solution (ΔH_{ds}) in lead borate, enthalpy of solution (ΔH_{soln}), and enthalpies of dehydration ($\Delta H_{dehydration}$) is shown in Table 6. The enthalpy of dehydration of sample S3 was calculated from the enthalpies of drop solution because the complete dehydration of the sample is insured in the drop solution experiments (all water is evolved from the melt into the gas phase). In contrast, the enthalpies of transposed temperature drop were not used because their values suggest that the dehydration of the sample may not have been complete.

Table 4 Literature heat of formation from elements of hematite and magnetite

Sample	ΔH_f^0 at 25°C/kJ mol^{-1}	ΔH_f^0 at 1353°C/kJ mol^{-1}	Reference
Hematite Fe_2O_3	–826.2±1.3	–805.2±1.3	[28]
Magnetite Fe_3O_4	–1115.7±2.1	–1082.9±2.1	[28]
ΔH_{rxn} (reduction)	247.2±2.5	249.8±2.5	Calculated

Table 5 Thermochemical cycle used to calculate the enthalpy of dehydration from iron ore sample

Reaction	Enthalpy
M.n (H_2O) (solid, 25°C) → M (soln, 702°C)+n(H_2O) (gas, 702°C)	$\Delta H_1=\Delta H_{ds}$ (M.n)
M (solid, 25°C) → M (soln, 702°C)	$\Delta H_2=\Delta H_{ds}$ (M)
H_2O (g, 25°C) → H_2O (gas, 702°C)	$\Delta H_3=\Delta H_{hc}$ (H_2O)*
M.n (H_2O) (solid, 25°C) → M (solid, 25°C)+n(H_2O) (g, 25°C)	$\Delta H_4=\Delta H_{Dehydration}$
ΔH of dehydration=$\Delta H_4=\Delta H_1-\Delta H_2-n\Delta H_3$	

where 1 mol of M is defined as $(Fe_2O_3)_{0.836}(CaO)_{0.001}(SiO_2)_{0.138}(Al_2O_3)_{0.022}(MgO)_{0.002}$ has 144.24 g mol^{-1}
where 1 mol of M.n is defined as M+$(H_2O)_{0.861}$ has 159.74 g mol^{-1}
where n is 0.861, *from Robie and Hemingway where ΔH_{hc} (H_2O)=26.04 kJ mol^{-1}

Table 6 Enthalpies of transposed temperature drop (TTD) (ΔH_{TTD}) and enthalpies of drop solution (ΔH_{ds}) calorimetry in lead borate, enthalpy of solution (ΔH_{soln}) at 702°C, and calculated enthalpies of dehydration ($\Delta H_{Dehydration}$)

Sample	ΔH_{TTD}*/kJ mol^{-1}	ΔH_{ds}*/kJ mol^{-1}	ΔH_{soln}*/kJ mol^{-1}	$\Delta H_{Dehydration}$*/kJ mol^{-1}
S3 (M.n)	146.6±1.2 (6)	202.6±0.6 (6)	55.9±1.3	39.4±1.1
S3 (M)	95.6±0.8 (6)	140.8±0.9 (6)	45.2±1.2	

*Uncertainty is two standard deviations of the mean. The number in parentheses is the number of experiments

Sample	ΔH_{TTD}*/J g^{-1}	ΔH_{ds}*/J g^{-1}	ΔH_{soln}*/J g^{-1}
S3 (M.n)	917.6±7.4 (6)	1267.7±3.9 (6)	350.1±8.4
S3 (M)	662.8±5.3 (6)	976.31±6.0 (6)	313.5±8.0

Table 7 Thermochemical cycle for enthalpy of dehydration at 298 K, from the elements

Reaction	Enthalpy
2w FeOOH (solid, 25°C) → w Fe_2O_3(solid, 25°C)+w (H_2O) (gas, 25°C)	ΔH_1=w ΔH_f (Fe_2O_3)+w ΔH_f (H_2O)–2w ΔH_f (FeOOH)
x $Ca(OH)_2$ (solid, 25°C) → x CaO (solid, 25°C)+x H_2O (gas, 25°C)	ΔH_2=x ΔH_f (CaO)+x ΔH_f (H_2O)–x ΔH_f ($Ca(OH)_2$)
2y AlOOH (solid, 25°C) → y Al_2O_3 (solid, 25°C)+y H_2O (gas, 25°C)	ΔH_3=y ΔH_f (Al_2O_3)+y ΔH_f (H_2O)–2y ΔH_f (AlOOH)
z $Mg(OH)_2$ (solid, 25°C) → z MgO (solid, 25°C)+z H_2O (gas, 25°C)	ΔH_4=z ΔH_f (MgO)+z ΔH_f (H_2O)–z ΔH_f ($Ca(OH)_2$)
[w Fe_2O_3+x CaO+y Al_2O_3+z MgO+t SiO_2] (solid, 25°C)+(w+x+y+z) H_2O (gas, 25°C) → 2w FeOOH (solid, 25°C)+x $Ca(OH)_2$ (solid, 25°C)+2y AlOOH (solid, 25°C)+z $Mg(OH)_2$ (solid, 25°C)+t SiO_2 (solid, 25°C)	$\Delta H_5=\Delta H_1+\Delta H_2+\Delta H_3+\Delta H_4$

All of ΔH_f values are found in Table 8.

The enthalpy of dehydration can also be approximated from the composition of the oxides in iron ore, by using the appropriate thermochemical cycle (Table 7). Assuming SiO_2 is not hydrated, the calculated enthalpy of dehydration from the thermochemical cycle (based on heat of formation of the respective oxides (Table 8)) for samples S1–S5 yields 42 to 47 kJ mol^{-1} range (Table 9). The estimated enthalpy of dehydration of sample S3 (42.3±2.5 kJ mol^{-1} (Table 9)) is in agreement with the measured value (39.4±1.1 kJ mol^{-1} (Table 6)) and the results of previous studies (41.3–67.3 kJ mol^{-1}) [20, 26–28]. The measured dehydration enthalpy (39.4±1.1 kJ mol^{-1}) is actually very small in comparison to other endothermic process occurring during sintering such as the calcination of limestone used as flux (317.3±7.2 kJ mol^{-1}).

Table 8 Heat of formation from elements for several oxides found in iron ore samples

Sample	ΔH_f*/kJ mol^{-1}
Fe_2O_3	–826.2±1.3
H_2O (ideal gas)	–241.8±0.1
FeOOH	–558.1±1.3
CaO	–635.1±0.9
$Ca(OH)_2$	–986.1±1.3
Al_2O_3	–1675.7±1.3
AlO(OH)	–996.4±2.2
MgO	–601.6±0.3
$Mg(OH)_2$	–924.5±0.4

*Values obtained from Robie and Hemingway [28]

Table 9 Calculated enthalpy of dehydration from iron ore composition using thermochemical cycle in Table 7

	1 mol=$(Fe_2O_3)_w$ $(CaO)_x$ $(Al_2O_3)_y$ $(MgO)_z$ $(SiO_2)_t$ $(H_2O)_{w+x+y+z}$						
Sample	*w*	*x*	*y*	*z*	*t*	*w*+*x*+*y*+*z*	$\Delta H_{Dehydration}$ /kJ mol^{-1*}
S1	0.859	0.002	0.032	0.004	0.103	0.897	44.4±2.5
S2	0.888	0.0003	0.029	0.002	0.079	0.919	45.3±2.5
S3	0.836	0.001	0.022	0.002	0.138	0.861	42.3±2.5
S4	0.834	0.006	0.028	0.002	0.130	0.870	43.2±2.5
S5	0.948	0.001	0.017	0.001	0.033	0.967	47.2±2.5

*Uncertainty is two standard deviations of the mean.

Conclusions

By using differential scanning and high-temperature reaction calorimetry, the thermochemistry of some fundamental processes occurring during sintering of iron ores, have been examined. In order to understand the energy required to assimilate an iron ore particle during sintering, drop solution and transposed temperature drop calorimetry have been used to measure the energetics of primary melt formation. There is no concentration dependence of the heat of solution of common iron ores in the iron rich melts. The heat content for several sinter samples was measured and showed no dependence on the Fe_2O_3 content. The volatile content, evolution of water, and/or carbon dioxide, and enthalpy of dehydration ΔH_{trns} of goethite to hematite of several iron ore samples were measured by DSC/TG.

Acknowledgements

The authors gratefully acknowledge valuable discussion with Dr. Benjamin G. Ellis.

References

1 P. R. Dawson, J. Ostwald and K. M. Hayes, Transactions of the Institution of Mining and Metallurgy Section C-Mineral Processing and extractive Metallurgy, 94 (1985) C71–78.
2 T. Kawaguchi and T. Usui, ISIJ Int., 45 (2005) 414.
3 C. E. Loo and W. Leung, ISIJ Int., 43 (2003) 1393.
4 M. Gabal, D. Hoff and G. Kasper, J. Therm. Anal. Cal., 89 (2007) 27.
5 M. Laskou and G. Margomenou-Leonidopoulou, J. Therm. Anal. Cal., 84 (2006) 141.
6 S. Sarkar, S. Ray and I. Chatterjee, J. Therm. Anal. Cal., 35 (1989) 2461.
7 A. Navrotsky, Phys. Chem. Miner., 24 (1997) 222.
8 A. Navrotsky, D. Ziegler, R. Oestrike, and P. Maniar, Contributions Mineral. Petrology, 101 (1989) 122.
9 M. Wilding and A. Navrotsky, Neues Jahrbuch für Mineralogie Abhandlungen, 172 (1998) 177.
10 M. Wilding and A. Navrotsky, J. Non-Cryst. Solids, 265 (2000) 238.
11 ICSD, Inorganic Crystal Structure Database, Institute of Standards and Technology 2004, Version 1.3.4.
12 R. Lange and A. Navrotsky, Contrib. Mineral. Petrol., 110 (1992) 311.
13 D. Ziegler and A. Navrotsky, Geochim. Cosmochim. Acta, 50 (1986) 2461.
14 R. Morcos, B. Ellis and A. Navrotsky, Am. Mineral., 92 (2007) 92.
15 B. Ellis, R. Morcos and A. Navrotsky, International Conference on Science & Technology of Ironmaking, The 4th International Congress on the Science and Technology of Ironmaking (ICSTI '06) 2006, (Osaka), pp. 651–654.
16 M. Morishita, A. Navrotsky and M. Wilding, J. Am. Ceram. Soc., 87 (2004) 1550.
17 A. Navrotsky, Phys. Chem. Miner., 2 (1977) 89.
18 R. M. Morcos, Energetics of nanostructured, amorphous, and molten materials related to technology. In [Online] University of California, Davis: Davis, 2007; pp. 434, AAT 3283008.
19 E. Kasai, Y. Waseda and M. V. Ramos, Testu to Hagane. 83 (1997) 539.
20 D. Walter, G. Buxbaum and W. Laqua, J. Therm. Anal. Cal., 63 (2001) 733.
21 E. Fluck, J. Res. National Institute Standards Technol., 101 (1996) 217.
22 JADE, in Materials Data Inc., 2002.
23 M. D. Alcala, J. M. Criado, C. Real, T. Grygar, M. Nejezchleba, J. Subrt and E. Petrovsky, J. Mater. Sci., 39 (2004) 2365.
24 M. S. Ellid, Y. S. Murayed, M. S. Zoto, S. Music and S. Popovic, J. Radioanal. Nuclear Chem., 258 (2003) 299.
25 E. Petrovsky, M. D. Alcala, J. M. Criado, T. Grygar, A. Kapicka and J. Subrt, J. Magn. Magn. Mater., 210 (2000) 257.
26 A. Florindi, M. Petroni and M. Pelino, Thermochim. Acta, 138 (1989) 47.
27 M. Pelino, L. Toro, M. Petroni, A. Florindi and C. Cantalini, J. Mater. Sci., 24 (1989) 409.
28 R. A. Robie and B. S. Hemingway, U. S. Geological Survey Bull., 2131 (1995) 192.

Received: September 25, 2007
Accepted: June 30, 2008
Online First: January 12, 2009

DOI: 10.1007/s10973-008-8783-y